Global urban population exposure to extreme heat

Cascade Tuholske[a,b,c,1], Kelly Caylor[a,d], Chris Funk[a,b], Andrew Verdin[e], Stuart Sweeney[a], Kathryn Grace[e,f], Pete Peterson[b], and Tom Evans[g]

[a]Department of Geography, University of California, Santa Barbara, CA 93106; [b]Climate Hazards Center, University of California, Santa Barbara, CA 93106; [c]Center for International Earth Science Informational Network, The Earth Institute, Columbia University, New York, NY 10964; [d]Bren School of Environmental Science & Management, University of California, Santa Barbara, CA 93106; [e]Minnesota Population Center, University of Minnesota, Twin Cities, Minneapolis, MN 55455; [f]Department of Geography, Environment & Society, University of Minnesota, Twin Cities, Minneapolis, MN 55455; and [g]School of Geography, Development and Environment, University of Arizona, Tucson, AZ 85719

Edited by Matei Georgescu, Arizona State University, Tempe, AZ, and accepted by Editorial Board Member Susan Hanson June 22, 2021 (received for review December 3, 2020)

Increased exposure to extreme heat from both climate change and the urban heat island effect—total urban warming—threatens the sustainability of rapidly growing urban settlements worldwide. Extreme heat exposure is highly unequal and severely impacts the urban poor. While previous studies have quantified global exposure to extreme heat, the lack of a globally accurate, fine-resolution temporal analysis of urban exposure crucially limits our ability to deploy adaptations. Here, we estimate daily urban population exposure to extreme heat for 13,115 urban settlements from 1983 to 2016. We harmonize global, fine-resolution (0.05°), daily temperature maxima and relative humidity estimates with geolocated and longitudinal global urban population data. We measure the average annual rate of increase in exposure (person-days/year^{-1}) at the global, regional, national, and municipality levels, separating the contribution to exposure trajectories from urban population growth versus total urban warming. Using a daily maximum wet bulb globe temperature threshold of 30 °C, global exposure increased nearly 200% from 1983 to 2016. Total urban warming elevated the annual increase in exposure by 52% compared to urban population growth alone. Exposure trajectories increased for 46% of urban settlements, which together in 2016 comprised 23% of the planet's population (1.7 billion people). However, how total urban warming and population growth drove exposure trajectories is spatially heterogeneous. This study reinforces the importance of employing multiple extreme heat exposure metrics to identify local patterns and compare exposure trends across geographies. Our results suggest that previous research underestimates extreme heat exposure, highlighting the urgency for targeted adaptations and early warning systems to reduce harm from urban extreme heat exposure.

climate change | hazards | public health | sustainability | urbanization

Increased exposure to extreme heat from both climate change (1–5) and the urban heat island (UHI) effect (6–9) threaten the sustainability of rapidly growing urban settlements worldwide. Exposure to dangerously high temperatures endangers urban health and development, driving reductions in labor productivity and economic output (10, 11) and increases in morbidity (1) and mortality (2, 3, 12). Within urban settlements, extreme heat exposure is highly unequal and most severely impacts the urban poor (13, 14). Despite the harmful and inequitable risks, we presently lack a globally comprehensive, fine-resolution understanding of where urban population growth intersects with increases in extreme heat (2, 6, 15). Without this knowledge, we have limited ability to tailor adaptations to reduce extreme heat exposure across the planet's diverse urban settlements (6, 15, 16).

Reducing the impacts of extreme heat exposure to urban populations requires globally consistent, accurate, and high-resolution measurement of both climate and demographic conditions that drive exposure (5, 15, 17). Such analysis provides decision makers with information to develop locally tailored interventions (7, 18, 19) and is also sufficiently broad in spatial coverage to transfer knowledge across urban geographies and climates (6). Information about exposures and interventions from diverse contexts is vital for the development of functional early warning systems (20) and can help guide risk assessments and inform future scenario planning (21). Existing global extreme heat exposure assessments (1, 2), however, do not meet these criteria (*SI Appendix*, Table S1) and are insufficient for decision makers. These studies are coarse grained (>0.5° spatial resolution), employ disparate or single metrics that do not capture the complexities of heat-health outcomes (22), do not separate urban from rural exposure (19), and rely on climate reanalysis products that can be substantially (~1 to 3 °C) cooler than in situ data observations (5, 23, 24). In fact, widely cited benchmarks (25) that estimate extreme heat with the version 5 of the European Centre for Medium-Range Weather Forecasts Reanalysis (ERA5) (26) may greatly underestimate total global exposure to extreme heat (5, 23, 24). Using a 40.6 °C daily maximum 2-m air temperature threshold (T_{max}), recent analysis found that ERA5 T_{max} drastically underestimated the number of extreme heat days per year compared to in situ observations (23). Finally, few studies (2, 18) have assessed urban extreme heat exposure across data-sparse (23) rapidly urbanizing regions, such as sub-Saharan Africa, the Middle East, and Southern Asia (27), that may be most impacted by increased extreme heat events due to climate change (3, 5, 28).

Here, we present a globally comprehensive, fine-resolution, and longitudinal estimate of urban population exposure to extreme

Significance

Increased extreme heat exposure from both climate change and the urban heat island effect threatens rapidly growing urban settlements worldwide. Yet, because we do not know where urban population growth and extreme heat intersect, we have limited capacity to reduce the impacts of urban extreme heat exposure. Here, we leverage fine-resolution temperature and population data to measure urban extreme heat exposure for 13,115 cities from 1983 to 2016. Globally, urban exposure increased nearly 200%, affecting 1.7 billion people. Total urban warming elevated exposure rates 52% above population growth alone. However, spatially heterogeneous exposure patterns highlight an urgent need for locally tailored adaptations and early warning systems to reduce harm from urban extreme heat exposure across the planet's diverse urban settlements.

Author contributions: C.T., K.C., C.F., and S.S. designed research; C.T., K.C., C.F., A.V., and P.P. performed research; C.T., K.C., C.F., A.V., and P.P. contributed new reagents/analytic tools; C.T., K.C., C.F., A.V., S.S., K.G., and T.E. analyzed data; and C.T., K.C., C.F., A.V., K.G., S.S., and T.E. wrote the paper.

The authors declare no competing interest.

This article is a PNAS Direct Submission. M.G. is a guest editor invited by the Editorial Board.

[1]To whom correspondence may be addressed. Email: cascade@ucsb.edu.

This article contains supporting information online at https://www.pnas.org/lookup/suppl/doi:10.1073/pnas.2024792118/-/DCSupplemental.

Published October 4, 2021.

heat—referred to henceforth as exposure—for 13,115 urban settlements from 1983 to 2016. To accomplish this, we harmonize global, fine-grained (0.05° spatial resolution) T_{max} estimates (23) with global urban population and spatial extent data (29). For each urban settlement, we calculate area-averaged daily wet bulb globe temperature ($WBGT_{max}$) (30) and heat index (HI_{max}) (31) maxima using Climate Hazards Center InfraRed Temperature with Stations Daily (CHIRTS-daily) T_{max} (23) and down-scaled daily minimum relative humidity (RH_{min}) estimates (32). CHIRTS-daily is better suited to measure urban extreme heat exposure than other gridded temperature datasets used in recent global extreme heat studies (*SI Appendix*, Table S1) for two reasons. First, it is more accurate, especially at long distances (refer to figure 3 in ref. 23), than widely used gridded temperature datasets to estimate urban temperature signals worldwide (*SI Appendix*, Figs. S1 and S2). Second, it better captures the spatial heterogeneity of T_{max} across diverse urban contexts (*SI Appendix*, Fig. S3). These factors are key for measuring extreme heat exposure in rapidly urbanizing, data-sparse regions.

As discussed in refs. 23 and 24, the number of in situ temperature observations is far too low across rapidly urbanizing (27) regions to resolve spatial and temporal urban extreme heat fluctuations, which can vary dramatically over small distances and time periods. For example, of the more than 3,000 urban settlements in India (29), only 111 have reliable station observations (*SI Appendix*, Fig. S3). While climate reanalyses can help overcome these limitations, they are coarse grained (*SI Appendix*, Table S1) and suffer from mean bias, and, to a lesser degree, temporal fidelity. ERA5 has been shown to substantially underestimate the increasing frequencies of heat extremes (figure 4 in ref. 23), while Modern-Era Retrospective analysis for Research and Applications Version 2 (MERRA2) fails to represent the substantial increase in recent monthly T_{max} values (figure 8 in ref. 24). These datasets dramatically underestimate increases in warming. CHIRTS-daily overcomes these limitations by coherently stacking information from a high-resolution (0.05°) climatology-derived surface emission temperature (24), interpolated in situ observations, and ERA5 reanalysis to produce a product that has been explicitly developed to monitor and assess temperature related hazards (23). As such, CHIRTS-daily is best suited to capture variation in exposure across urban settlements in rapidly urbanizing (27), data-sparse regions such as sub-Saharan Africa, the Middle East, and Southern Asia (*SI Appendix*, Fig. S3) (24).

We measure exposure in person-days/year^{-1}—the number of days per year that exceed a heat exposure threshold multiplied by the total urban population exposed (5). We then estimate annual rates of increase in exposure at the global (Fig. 1), regional (*SI Appendix*, Table S2), national (*SI Appendix*, Table S3), and municipality levels from 1983 to 2016 (*SI Appendix*, Table S4). At each spatial scale, we separate the contribution to exposure trajectories from total urban warming and population growth (5). For clarity, total urban warming refers to the combined increase of extreme heat in urban settlements from both the UHI effect and anthropogenic climate change. We do not decouple these two forcing agents (33, 34). However, we identify which urban settlements have warmed the fastest by measuring the rate of increase in the number of days per year that exceed the two extreme heat thresholds described below (15). Our main findings use an extreme heat exposure threshold defined as $WBGT_{max} > 30$ °C, the International Standards Organization (ISO) occupational heat stress threshold for risk of heat-related illness among acclimated persons at low metabolic rates (100 to 115 W) (30). $WBGT_{max}$ is a widely used heat stress metric (35) that captures the biophysical response (36) of hot temperature–humidity combinations (3, 17) that reduce labor output (36), lead to heat-related illness (36), and can cause death (23). In using a threshold $WBGT_{max} > 30$ °C, which has been associated with higher mortality rates among vulnerable populations (37), we aim to identify truly extremely hot temperature–humidity combinations (17) that can harm human health and well-being. We recognize, however, that strict exposure thresholds do not account for individual-level risks and vulnerabilities related to acclimatization, socio-economic, or health status or local infrastructure (18, 19, 38). We also note that there are a range of definitions of exposure, and we provide further analysis identifying 2-d or longer periods during which the maximum heat index (HI_{max}) (31) exceeded 40.6 °C (*SI Appendix*, Figs. S4–S6) following the US National Weather Service's definition for an excessive heat warning (39).

Results and Discussion

Global exposure increased 199% in 34 y, from 40 billion person-days in 1983 to 119 billion person-days in 2016, growing by 2.1 billion person-days/yr^{-1} (Fig. 1*A*). Population growth (Fig. 1*B*) and total urban warming (Fig. 1*C*) contributed 66% (1.5 billion person-days/yr^{-1}) and 34% (0.7 billion person-days/yr^{-1}) to the annual rate of increase in exposure, respectively. That is, total urban warming elevated the global annual rate of increase in exposure by 52% compared to urban population growth alone. This finding is not directly comparable to recent global benchmarks and projections of total population exposure to extreme heat because of disparate exposure definitions employed (*SI Appendix*, Table S1). However, our results indicate much higher

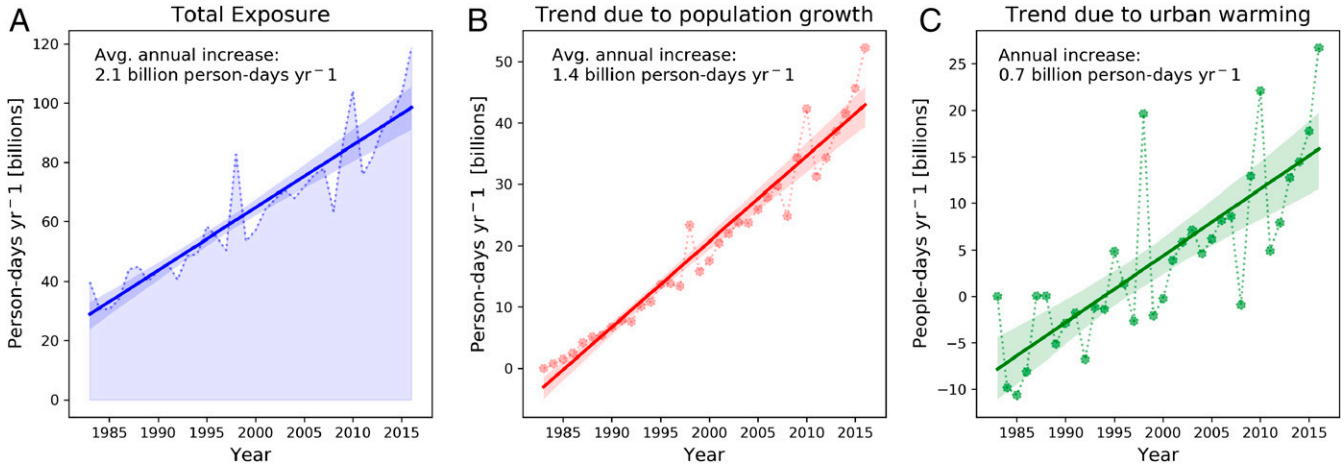

Fig. 1. Global urban population exposure to extreme heat, defined by 1-d or longer periods when $WBGT_{max} > 30$ °C, from 1983 to 2016 (*A*), with the contribution from population growth (*B*), and total urban warming (*C*) decoupled.

exposure rates compared to recent continental-scale benchmarks. Defining exposure as the total population multiplied by the number of days per year when $HI_{max} > 40.6$ °C, a recent study found that the total annual average exposure from 1986 to 2005 for 173 African cities was 4.2 billion person-days/yr^{-1} (40). When we apply the same exposure criteria to our data, including parameterizing HI_{max} with daily average RH instead of RH_{min}, we find six times the average total exposure for Africa, or 27.5 billion person-days/yr^{-1}, over the same time period. This contrasting exposure estimate showcases how the increased spatial and temporal accuracy of CHIRTS-daily T_{max} (*SI Appendix*, Figs. S1–S3), combined with the increased granularity of urban settlement data we employ (29), can better capture exposure trends in data-sparse regions like Africa.

While just 25 urban settlements contributed nearly 25% of the global annual rate of increase in exposure (*SI Appendix*, Table S3), we identify statistically significant ($P < 0.05$) positive-exposure trajectories from 1983 to 2016 for 46% (5,985) of municipalities worldwide (Fig. 2*A*). Together, these urban settlements comprised 23% of the planet's total population (27), or 1.7 billion people, in 2016 (27). The majority are concentrated in low latitudes but span a range of climates. Additionally, 17% (2,252) of urban settlements added at least one day per year when $WBGT_{max}$ exceeded 30 °C (Fig. 2*B*). In other words, these urban settlements experienced an additional month of extreme heat in 2016 compared to 1983. Remarkably, 21 urban settlements with populations greater than 1 million residents in 2016 added more than 1.5 d per year of extreme heat. This includes Kolkata, India, which is the capital of the state of West Bengal and housed 22 million people in 2016 (29). These findings suggest that increased extreme heat is potentially elevating mortality rates for many of the planet's urban settlements, especially among those most socially and economically marginalized (37). Globally, for every additional day that T_{max} exceeds 35 °C compared to 20 °C, mortality increases by 0.45 per 100,000 people, with an increase of 4.7 extra deaths per 100,000 people for those above 64 y old (12).

Separating the contribution to exposure trajectories from urban population growth and total urban warming underscores how the level of analysis affects our understanding of the spatial distribution and magnitude of exposure. The level of analysis employed can either mask or highlight spatial and temporal patterns that are key to allocating limited resources for adaptations and sharing knowledge across urban contexts (2, 5–7). Broadly, we find that municipality-level exposure trajectories (Fig. 2*C*) reflect national- and regional-level urbanization trends (27). In regions with slower urban population growth (27), like Latin America and the Caribbean (Fig. 3*A*) (27), the contribution of total urban warming to increases in exposure trajectories compared to urban population growth is largely responsible for increased exposure for the majority of municipalities compared to regions with more rapid urban population growth. As urban population growth rates increase by region, the signal from total urban warming diminishes for most municipalities, as evident by Western Asia (Fig. 3*B*), Southern Asia (Fig. 3*C*), and sub-Saharan Africa (Fig. 3*D*).

However, we detail striking spatial heterogeneity in how urban demographic and total urban warming signals drive exposure trajectories for individual municipalities (Fig. 2*C*), even those with similar population sizes and within the same country. As such, regional- and national-level assessments designed to inform policy implementation (1, 41) may fail to capture municipality-level (and finer-scale) nuances that are key for adaptations (7, 15) and future climate change scenario planning (21) (*SI Appendix, Supplementary Text* and Figs. S7 and S8). For example, in West Africa, while we find exposure trajectories increased for 88% of Nigerian urban settlements, the disparate influence of total urban warming across urban settlements may be dictated by local climate (*SI Appendix, Supplementary Text* and Fig. S8). Furthermore, we map pockets of urban settlements in Southern India, the Ganges Delta, the Nile river valley and delta, and along the Tigris–Euphrates (Fig. 2*C* and *SI Appendix*, Fig. S9)—all rapidly urbanizing regions (1)—where total urban warming exceeded urban population growth as the driver of exposure. This geographic pattern parallels recent global analysis of station observations of extreme humid heat that suggest areas of the planet may soon exceed human biophysical capacity, regardless of local acclimatization (17).

Among the clearest examples of the importance of differentiating urban demographic and total urban warming signals at the municipality level are two Indian megacities: Delhi and Kolkata. Exposure trajectories for both cities are congruent (*SI Appendix*, Table S4 and Fig. S10*A*). However, population growth contributed to nearly 75% of the increase in Delhi's exposure trajectory, whereas population growth accounted for only 48% of the annual rate of increase in exposure in Kolkata (*SI Appendix*, Table S4 and Fig. S10 *B* and *C*). The stark contrast in the impact of total urban warming versus urban population growth on the two cities' exposure trajectories (*SI Appendix*, Fig. S10) reinforces that individual adaptations require fine-grained spatiotemporal yet globally comparable analysis (6, 15). Such precision is crucial for decision makers given the range of adaptation choices and costs (7, 15) and also opens avenues of inquiry to examine linkages between elevated temperatures, changes in humidity, and drivers of urban population growth (16, 42–45).

Finally, while our main findings focus on exposure determined by $WBGT_{max} > 30$ °C, we showcase the contrast between $WBGT_{max}$ and HI_{max} exposure estimates with two examples of poorly documented local urban extreme heat events. First, air temperatures that reached 49.8 °C reportedly killed thousands of people in India in 1998 (46). However, the reports do not specify nor identify impacts specific to urban settlements. In Kolkata, which was home to 12 million people in 1998 (27), we find that HI_{max} exceeded 40.6 °C for 53 consecutive days in May through June 1998 (Fig. 4*A*). During this period, the average HI_{max} exceeded the 34-y daily HI_{max} average by as much as 9 °C (27). The amplitude of daily extreme temperature–humidity combinations, however, is not resolved using $WBGT_{max}$ (Fig. 4*B*), because $WBGT_{max}$ saturates at high values (47).

Next, we examine the summer of 2010 in Syria, which was the final year of a 4-y drought that was two to three times more likely because of climate change (48). In Aleppo, home to 3 million people in 2010 (27), we document an 8-d period shortly followed by a 7-d period with HI_{max} above 40.6 °C (Fig. 4*C*). We isolate the peak of the heat wave hitting Aleppo on Aug. 5, during which HI_{max} exceeded 47 °C (9 °C above average HI_{max} for Aug. 5) and marked the second-hottest day in the entire 34-y record. Yet, like Kolkata in 1998, the amplitude of the extreme heat events in Aleppo in 2010 is not captured by $WBGT_{max}$ compared to HI_{max} (Fig. 4*D*). While the likelihood of heat waves has increased for the Eastern Mediterranean since the 1960s (49), to our knowledge, urban extreme heat during the summer of 2010 in Syria has not been documented nor quantified until now. This extreme heat event occurred 6 mos prior to the beginning of the Syrian uprising. While conflict and climate linkages are inconclusive and complex (50, 51), this finding from Aleppo illustrates potential advantages of higher-resolution data and analysis we present here for future research to examine climate–conflict linkages.

We present these examples not to advocate for or against the use of either $WBGT_{max}$ or HI_{max} to measure exposure. Both have limitations when independently used to quantify extreme heat exposure. HI_{max} was not intended to estimate heat exposure above $HI_{max} \sim 50$ °C (52), and the second order power function that we used to convert HI_{max} to $WBGT_{max}$ explains the asymptotic ceiling of $WBGT_{max}$ and its failure to capture daily extremes like HI_{max} does (47). Rather, we join the growing community of scholars advocating for the use of multiple (22) place-based heat wave metrics that inform and create better synergies across research domains (19). Locally-defined exposure criteria (18) are especially useful for early warning systems (53) when tied to biophysical

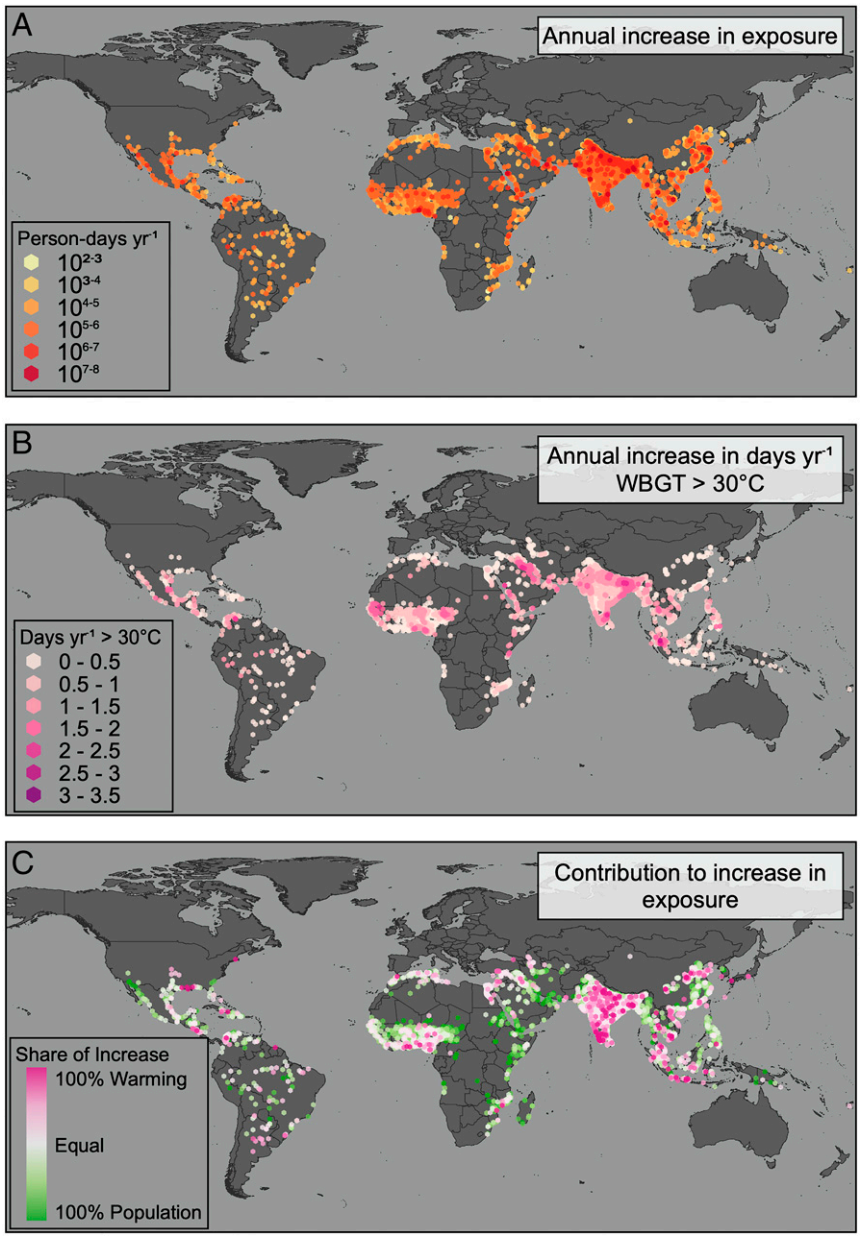

Fig. 2. (*A*) Municipality-level increase in the rate of urban population exposure to extreme heat from 1983 to 2016 and (*B*) the rate of increase in the total number of days per year when $WBGT_{max}$ > 30 °C. (*C*) The share of population versus total urban warming in the rate of increase of total population exposure using $WBGT_{max}$ > 30 °C. *SI Appendix*, Fig. S4 zooms in on Southern India, Ganges Delta, Nile river valley and delta, and Tigris–Euphrates river valley. Note, the largest increase in exposure (*A*) and days per year WBGT > 30 °C (*B*) are rendered last for emphasis. In *C*, urban settlements with a greater contribution from total urban warming (e.g., pink) are rendered last for emphasis.

response of extreme heat with impacts on individual-level human health and well-being (19, 22) as well as are comparable across geographies (6).

By focusing on extremely hot–humid exposure defined by >30 °C, our global synthesis of urban extreme heat exposure is conservative. For example, when we adjust the threshold to $WBGT_{max}$ > 28 °C (*SI Appendix*, Fig. S11), the ISO occupational standard risk for heat-related illness for acclimated people at moderate metabolic rates (235 to 360 W) (30), 7,628 urban settlements have a significant increase ($P < 0.05$) in exposure from 1983 to 2016 (*SI Appendix*, Fig. S11). In contrast, when we adjust the threshold to $WBGT_{max}$ > 32 °C, the ISO heat-risk threshold for unacclimated people at resting metabolic rates (100 to 125 W) (30), 2,979 urban settlements have a significant ($P < 0.05$) increase in exposure from 1983 to 2016 (*SI Appendix*, Fig. S11). Accordingly, our findings suggest that in already hot regions, like the Sun Belt Region in the United States, where air temperatures are projected to increase (18), temperature–humidity combinations may not regularly exceed extremes like $WBGT_{max}$ > 32 °C for many urban settlements. For example, take Phoenix, Arizona. The hottest T_{max} ever recorded in Phoenix was 122 °F on June 26, 1990, at 23 h Greenwich Mean Time (54, 55). The relative humidity at that time was 11% (54). Following our methods, the HI_{max} equivalent was 49 °C, and the equivalent $WBGT_{max}$ was 32.29 °C. Yet, vulnerable populations regularly experience extreme heat exposure in Phoenix (56, 57), demonstrating the need for diverse definitions of heat stress.

In sum, our analysis calls into question the future sustainability and equity for populations living in and moving to many of the

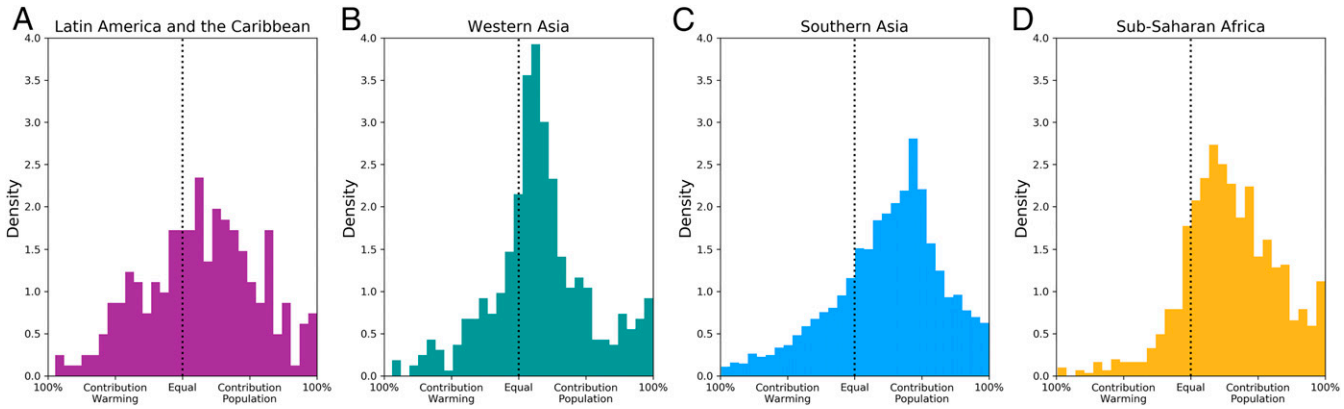

Fig. 3. Aggregated by region, the comparative contribution to the increase in the rate of urban exposure to extreme heat due to population growth versus total urban warming largely follows regional-level urban population growth rates as shown by the examples of (*A*) Latin America and the Caribbean, (*B*) Western Asia, (*C*) Southern Asia, and (*D*) Sub-Saharan Africa.

planet's urban settlements. Climate change is increasing the frequency, duration, and intensity of extreme heat across the globe (1–5). Indeed, combined temperature and humidity extremes already exceed human biophysical tolerance in some locations (17). Poverty reduction in urban settlements ultimately hinges on increasing labor productivity (10), but across spatial scales, elevated temperatures have been associated with decreased economic output (11, 58, 59). As such, the spatial pattern of exposure trajectories that we identify in Africa and Southern Asia, which already house hundreds of millions of the urban poor (60), highlight that without sufficient investment, humanitarian intervention, and government support, extreme heat may crucially limit the urban poor's ability to realize the economic gains associated with urbanization (61). Synthesizing extreme heat exposure across all individual urban settlements globally, however, reveals that exposure trajectories are composed of thousands of extreme heat events. Each of those events presents an opportunity for effective early warning, a tool that, if widely implemented, can reduce the burden extreme heat places on all urban populations (20).

Materials and Methods

Daily Temperature. CHIRTS-daily provides globally extensive, high-resolution (0.05°) daily maximum and minimum temperature estimates (T_{max} and T_{min}) from 1983 to 2016 (23). CHIRTS-daily T_{max} and T_{min} are produced by bias correcting ERA5 T_{max} data with the monthly averaged T_{max} from the Climate Hazards center InfraRed Temperature with Stations ($CHIRTS_{max}$) climate data record (24). By combining cloud-screened harmonized geostationary satellite thermal infrared observations with ~15,000 in situ station observations from Berkeley Earth (62), $CHIRTS_{max}$ is the most accurate (R^2 = 0.8 to 0.9) high-resolution, monthly maximum temperature dataset with global coverage (24). The advantage of $CHIRTS_{max}$ is that it captures T_{max} in rapidly urbanizing (27) yet data-sparse regions (*SI Appendix*, Figs. S1 and S2). Indeed, from 1983 to 2016, station-based daily observations of temperature maxima declined globally from 5,900 to 1,000 (24). This decline was especially acute in sub-Saharan Africa, the Middle East, and Southern Asia, regions that have the fastest-growing urban populations (27). Validation of CHIRTS-daily T_{max} against Global Historical Climatology Network and Global Summary of the Day databases show that CHIRTS-daily consistently outperforms the widely used Princeton University's Global Meteorological Forcing Dataset for land surface modeling (*SI Appendix*, Figs. S1–S3) (63) as well ERA5 (26).

The methodology used to produce the CHIRTS-daily T_{max} relies on fusing the skill of $CHIRTS_{max}$ at measuring high-spatial resolution monthly climatology (24) with the ability of ERA5 T_{max} to measure daily temperature anomalies. To produce CHIRTS-daily T_{max}, first, ERA5 T_{max} and T_{min} are down-scaled from 0.25° latitude by 0.25° longitude to 0.05° by 0.05° using bilinear interpolation to match the spatial resolution of $CHIRTS_{max}$. Next, the ERA5 daily diurnal temperature range (DTR) is calculated by subtracting ERA5 daily T_{max} from ERA5 daily T_{min} (DTR) (Eq. **1**). ERA5 daily T_{max} are then converted to anomalies by subtracting the ERA5 monthly T_{max} average from the daily ERA5 T_{max} value (Eq. **2**). The ERA5 T_{max} daily anomalies are then added to the $CHIRTS_{max}$ value for a given month (Eq. **3**). CHIRTS-daily T_{min} is produced by subtracting the ERA5 daily DTR from CHIRTS-daily T_{max} (Eq. **4**). This process is repeated across all months and all days from 1983 to 2016 and can be expressed as

$$\mathrm{DTR}_t = \mathrm{ERA5}T_{\mathrm{max}_t} - \mathrm{ERA5}T_{\mathrm{min}_t} \text{for } t = 1 \ldots T \quad [1]$$

$$\mathrm{ERA5}T^{m,\mathrm{anomn}}_{\mathrm{max}_t} = \mathrm{ERA5}T^{t}_{\mathrm{max}_t} - \mathrm{ERA5}T^{m}_{\mathrm{max}} \text{ for } t = 1 \ldots T, m = 1 \ldots M \quad [2]$$

$$\mathrm{CHIRTS}_{\mathrm{daily}}T_{\mathrm{max}} = \mathrm{CHIRTS}_{\mathrm{max}} + \mathrm{ERA5}T^{m,\mathrm{anomn}}_{\mathrm{max}_t} \quad [3]$$

$$\mathrm{CHIRTS}_{\mathrm{daily}}T_{\mathrm{min}} = \mathrm{CHIRTS}_{\mathrm{daily}}T_{\mathrm{max}} - \mathrm{DTR}_t, \quad [4]$$

where T is all the days (t) in the CHIRTS-daily record, and M is all the months (m) in the $CHIRTS_{max}$ record from 1983 to 2016.

Daily Relative Humidity Product. Because T_{max} generally occurs when RH is lowest during a diurnal cycle (32), daily RH_{min} are calculated (Eqs. **5** through **7**) by combining CHIRTS-daily T_{max} with down-scaled ERA5 dew-point pressure (T_d) and surface pressure (p, kg/kg) from MERRA-2. ERA5 T_d is down-scaled from 0.25° longitude by 0.25° latitude, and MERRA-2 p is down-scaled from 0.5° latitude × 0.625° longitude to CHIRTS-daily's 0.05° by 0.05° spatial resolution using bilinear interpolation. To calculate RH_{min} (64), first, we calculated specific humidity (q) as

$$q = (0.622 \times e) \div (p - (0.378 \times e)), \quad [5]$$

where vapor pressure in millibars (e) is

$$e = 6.112 \times \exp((17.67 \times T_d) \div (T_d + 243.5)). \quad [6]$$

Daily RH_{min} is then calculated as

$$\mathrm{RH}_{\mathrm{min}} = 0.263 \times p \times q \div (\exp((17.67(T - T_0) \div T - 29.65)), \quad [7]$$

where T is the CHIRTS-daily T_{max}, and T_0 is 273.15 to convert Kelvin to Celsius. The result is a fine-grain daily RH estimate for the entire planet from 1983 to 2016.

Population Data. We use population estimates and spatial boundaries for 13,115 urban settlements from the Global Human Settlement Layer Urban Centre Database (GHS-UCDB) released by the European Commission Joint Research Council in 2019 (29). Available as vector shapefiles, GHS-UCDB is derived from a gridded population-modeling framework that apportions finest-available census data to grid cells based on built environment detected in the Landsat archive (for a complete description, refer to ref. 29). GHS-UCDB populations are benchmarked for 1975, 1990, 2000, and 2015. To estimate populations for each GHS-UCDB polygon for each year from 1983 to 2016, we apply a stepwise linear interpolation to the 1975, 1990, 2000, and 2015 GHS-UCDB population estimates for each urban settlement.

GHS-UCDB is the only well-documented global, geo-located urban population and extent dataset. We recognize that strict definitions of urban populations often fail to capture the urban–rural continuum (65) nor the

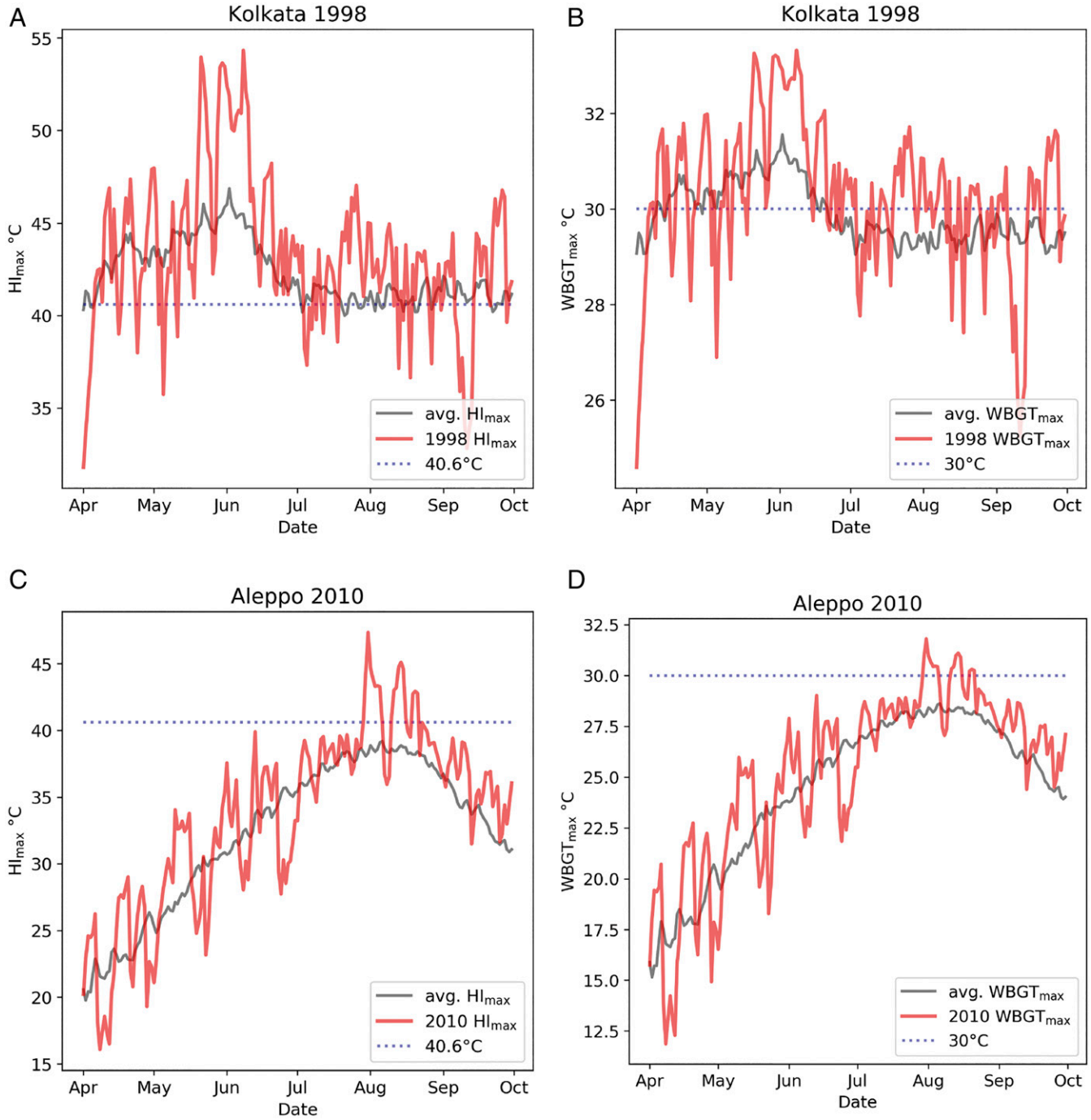

Fig. 4. Two examples—Kolkata, India, in 1998 (*A* and *B*) and Aleppo, Syria, in 2010 (*C* and *D*)—of previously poorly or undocumented documented urban heat waves that our analysis uncovered. In both cases, the contrast between daily HI_{max} (*A* and *C*) with $WBGT_{max}$ (*B* and *D*) estimates shows that while HI was not designed to be accurate at values $HI_{max} > 50$ °C, $WBGT_{max}$ does not capture the amplitude of daily extremely hot temperature–humidity combinations.

wide diversity and variation within and between urban settlements across the planet (66). However, by using a uniform criterion to identify populations and boundaries of urban settlements across the planet, the GHS-UCDB allows for direct comparison of urban settlements populations across disparate geographies and maps the diverse urban settlement patterns to strict fine-grained geographic boundaries requisite to calculating urban population exposure to extreme heat globally.

Overview of Data Harmonization. We convert the GHS-UCDB polygons to a raster in the same coordinate reference system (World Geodetic System 84) and spatial resolution as CHIRTS-daily T_{max} (0.05° by 0.05°). We then calculate HI_{max} and $WBGT_{max}$ with CHIRTS-daily T_{max} and RH_{min} for 0.05° pixels within each urban settlement from 1983 to 2016. For each urban settlement, we then area-average HI_{max} and $WBGT_{max}$ for each day in the data record. We recognize the limitations of using an area-average to characterize $WBGT_{max}$ and HI_{max} for an entire urban settlement, especially for large agglomerations that can span multiple climatic zones (6). However, robust global- and continental-scale urban heat studies report a single temperature for urban settlements (2, 3, 6). We also note that CHIRTS-daily is available at a finer spatial resolution (*SI Appendix*, Table S1) and has better spatial and temporal fidelity than the temperature datasets used in recent global retrospective and predictive extreme temperature studies (2, 3) and UHI effect studies (6).

Daily Urban Heat Index Maximum Estimates. We calculate daily HI_{max} for 0.05° pixels within each urban settlement following the National Ocean and Atmospheric Administration's (NOAA) guidelines (31). First, CHIRTS-daily T_{max} (referred to as T_{max} in Eqs. **8** through **11** for simplicity) and RH_{min} values are transformed from Celsius to Fahrenheit. Next, daily HI_{max} values are calculated using Steadman's equation and averaged with the T_{max}value (Eq. **8**):

$$HI_{max} = \frac{(0.5 \times (T_{max} + 61.0 + ((T_{max} - 68.0) \times 1.2) + (0.094RH_{min})) + T_{max}}{2}. \quad [8]$$

If the resulting averaged value is greater than 80 °F, we then calculate HI_{max} for each city following the complete Rothfusz equation (Eq. **9**):

$$\begin{aligned} HI_{max} = {} & -42.379 + 2.04901523T_{max} + 10.14333127RH_{min} \\ & - 0.22475541T_{max}RH_{min} - .00683783{T_{max}}^2 - 0.05481717{RH_{min}}^2 \\ & + 0.00122874{T_{max}}^2RH_{min} + 0.00085282T_{max}RH^2 \\ & - 0.00000199{T_{max}}^2{RH_{min}}^2. \end{aligned} \quad [9]$$

We then adjust the Rothfusz heat index values per NOAA's guidelines. For a given urban settlement on a given day, if T_{max} is between 80 and 112 °F and RH_{min} <13%, we subtract adjustment 1 from HI_{max} (Eq. **10**). If T_{max} is between 80 and 87 °F and RH_{min} > 85%, we add adjustment 2 to HI_{max} (Eq. **11**). We then convert all resulting maximum daily heat index values back to Celsius:

$$ADJ1 = \frac{0.25 \times (13 - RH_{min}) \times \sqrt{(17 - ABS(T_{max} - 95)}}{17}, \quad [10]$$

$$ADJ2 = \frac{RH_{min} - 85}{10} \times \frac{87 - T_{max}}{5}. \quad [11]$$

Daily Urban $WBGT_{max}$ Estimates. Pairwise HI_{max} and $WBGT_{max}$ values fit a second order power relationship, with HI_{max} estimates above 40.6 °C within ±0.5 °C of $WBGT_{max}$ (47), a more complex measure of extreme heat that incorporates radiant heat and air speeds and is widely used to measure occupational limits to heat stress (47). As such, we convert HI_{max} pixels estimates to $WBGT_{max}$ using Eq. **12**:

$$WBGT_{max}(°C) = -0.0034{HI_{max}}^2(°F) + 0.96HI_{max}(°F) - 34. \quad [12]$$

Urban Population Exposure to Extreme Heat. After area-averaging daily $WBGT_{max}$ and HI_{max} for each urban settlement from 1983 to 2016, we identify urban extreme heat events for two criteria: 1-d or longer periods in which $WBGT_{max}$ > 30 °C and 2-d or longer periods in which the maximum HI_{max} > 40.6 °C. The $WBGT_{max}$ threshold that we employ follows the ISO occupational heat stress criteria for risk of heat-related illness among acclimated people with low metabolic rates (125 to 180 W) (30, 36). The HI_{max} threshold follows the US National Weather Service's definition for an excessive heat warning (39). We acknowledge that the diversity of heat wave and extreme heat event definitions reflects the wide range of disciplines studying extreme heat (22). Climate scientists tend to use strict thresholds for comparable statistics across the planet, and physiologists and occupational health researchers tend to use thresholds tied to local adaptations connected to universal biophysical responses to heat stress (36). Rather than use percentile based criteria to identify heat stress that fit local contexts (18), we employ $WBGT_{max}$ and HI_{max} thresholds for two primary reasons: 1) to provide consistent estimates of urban extreme heat exposure trajectories that can be directly compared across urban geographic and spatial scales and 2) to capture the contribution to exposure trajectories from both urban population growth and total urban warming using thresholds that have been shown to impact human health and well-being.

Furthermore, unlike extreme heat studies that solely employ 2-m air temperature (1), both $WBGT_{max}$ and HI_{max} account for the nonlinear biophysical response to the relationship between humidity and air temperature (2). Core body temperatures are almost universally maintained around 37 °C and skin temperatures around 35 °C (67). Hyperthermia, elevated core body temperature, occurs when elevated skin temperatures are sustained, which can result in death when core body temperatures reach around 42 to 43 °C (68). While acclimatization can reduce the burden of heat (67, 69), acclimatization only improves sweating mechanisms, and the cooling effects of acclimated people have limits. As relative humidity increases, the evaporative cooling effects of sweating decreases, and once relative humidity reaches 100%, sweating continues but evaporative cooling stops. Even acclimated or healthy humans face mortality with prolonged skin temperatures of 37 to 38 °C (70, 71). Thus, it is reasonable that sustained periods of time with HI > 35 °C (72) can be physically intolerable, and outdoor exposure to $WBGT_{max}$ > 30 °C has been associated with increased mortality rates among vulnerable populations (37). Accordingly, our exposure thresholds are a conservative estimator yet comparable globally across spatial scales of urban population exposure to extreme heat to capture the harmful social (73), health (1), economic (11, 12), and potential political consequences (74) of exposure to extreme heat.

Urban Population Exposure Trends. We quantify urban exposure to extreme heat in person-days/year^{-1} for each GHS-UCDB urban settlement from 1983 to 2016. Person-days/year^{-1} is a widely used metric to compare and contrast exposure to extreme heat across geographies and time periods (3, 40, 75). For a given year (Y_i) and for a given urban settlement (j), we multiply the urban settlement's population (N_{ij}) by the number of days for year i that a threshold is exceeded (e.g., $WBGT_{max}$ > 30 °C, $Days_{ij}$; Eq. **13**).

After summing exposure in person-days/year^{-1} for each year at municipality, national, regional, and global scales, we evaluate annual rate of increase in exposure from 1983 to 2016 (person-days/year^{-1}) across spatial scales by fitting simple ordinary least squares linear regression models (OLS). For example, at the municipality level, we estimate the rate of change (β_{exp}) from 1983 to 2016 in person-days/year^{-1} as exposure (Exp_{ij}) for year i from 1983 to 2016 with Eq. **14**.

$$Exp_{ij} = N_{ij} \times Days_{ij}, \quad [13]$$

$$Exp_{ij} = \beta_0 + \beta_{exp}Y_i + \varepsilon. \quad [14]$$

Next, we fit simple OLS regression models to estimate the rate of change in the number of days per year when a threshold is exceeded for each urban settlement (Eq. **15**). For both the rates of increase in exposure and days per year that a threshold is exceeded, we subset the data to include only urban settlements with statistically significant positive trends ($P < 0.05$):

$$Warming_{ij} = \beta_0 + \beta_{j-days}Y_i + \varepsilon. \quad [15]$$

Contribution to Exposure from Population Growth versus Total Urban Warming. We quantify the share of exposure from population growth versus total urban warming for each urban settlement. For a given year i and urban settlement j, the share of person-days/year^{-1} from total urban warming ($Heat_{ij}$) is calculated by multiplying the urban settlement's population fixed at 1983 by the number of days per year that a threshold is exceeded (Eq. **16**):

$$Heat_{ij} = N_{83j} \times Days_{ij}. \quad [16]$$

The share of exposure from population is calculated by multiplying $Days_{ij}$ by the increase in population since 1983 (Eq. **17**):

$$Pop_{ij} = (N_{ij} - N_{83j}) \times Days_{ij}. \quad [17]$$

To measure the rate of change in $Heat_{ij}$and Pop_{ij}, we apply simple OLS regressions to estimate the average rate of increase in person-days/year^{-1}. The resulting coefficients, β_{pop} and β_{heat}, are the average rate of change in person-days/year^{-1} from total urban warming and population growth, respectively. We use these coefficients to generate a bounded index to measure the relative share in the increase of exposure from urban population growth versus total urban warming from 1983 to 2016. To this end, for a given urban settlement j, we subtract the rate of person-day increase from population growth (β_{pop}) from the rate of person-day increase due to warming (β_{heat}) and divide the result by the annual increase in coefficient of exposure (β_{exp}, Eq. **18**). We then normalize the index and plot the distribution of this index for at for all municipalities (Fig. 2*C* and *SI Appendix*, Fig. S5*C*) and by region (Fig. 3 and *SI Appendix*, Fig. S6):

$$Index = \left(\beta_{pop} - \beta_{heat}\right) \div \beta_{exp}. \quad [18]$$

Identifying Heat Waves. Our dataset includes more than 150 million area-averaged daily $WBGT_{max}$ and HI_{max} observations spanning more than 13,000 urban settlements from 1983 to 2016. As such, we produced a comprehensive inventory of urban extreme heat events across the two thresholds employed, for all urban settlements as a derivative product that identifies the duration, intensity, magnitude, and dates of all urban extreme heat events worldwide from 1983 to 2016. The entire dataset is searchable by English-language municipality names, country, and region (including sub- and

SUSTAINABILITY SCIENCE

intermediate-regions) and made publicly available (76) for scholars and practitioners to identify extreme heat events based on the criteria of their choosing (22).

Uncertainty and Limitations. We recognize that aside from our linear regression models, the results are presented as point estimates without uncertainty. Yet, all of the underlying data are from complex fusions of various different data sources. The underlying data products being used lack characterization of uncertainty and thus prevent us from estimating uncertainty in our results. Because of this, our analysis focuses on distinct and extreme differences in the patterns that we identify that are representative estimates of the true signals of the underlying processes. Given the fine-grained spatiotemporal resolution of our analysis, our results provide crucial improvements of previous coarse-scale data on total urban warming (3, 40) and urban population growth trends (27) that are key for future climate change scenario planning (21), adaptation development (6), and early warning system development (20).

Data Availability. The code produced for this anlaysis is publicly available on GitHub: https://github.com/ecohydro/GlobalUrbanHeat. The datasets used in this analysis are publicly available from the NASA Socioeconomic Data and Applications Center (SEDAC): https://doi.org/10.7927/fq7g-ny13 (76). CHIRTS-daily T_{max} and the relative humidity product are available from the University of California, Santa Barbara Climate Hazard Center: https://doi.org/10.15780/G2008H. GHS-UCDB is available from the European Commission Joint Research Centre: https://ghsl.jrc.ec.europa.eu/datasets.php.

ACKNOWLEDGMENTS. We would like to thank Prof. Susan Cassels for providing an internal review of this manuscript and the Earth Research Institute computing staff for their tireless assistance throughout this project. We also thank two anonymous reviewers, guest editor, and NAS board member for their excellent feedback. C.T. was supported by the University of California Presidential Dissertation Year Fellowship through UC Santa Barbara and the Earth Institute Postdoctoral Fellowship Program, Columbia University. C.T., K.C., and T.E. received support from NSF Awards SES-1801251 and SES-1832393. K.C. and T.E. recieved support from NSF Award DEB-1924309. Support for C.F. and P.P. came from the NASA Global Precipitation Measurement mission Grant 80NSSC19K0686, the US Agency for International Development cooperative agreement 72DFFP19CA00001, and the Famine Early Warning Systems Network and the Defense Advanced Research Projects Agency World Modelers Program under Army Research Office prime contract No. W911NF-18-1-0018.

1. N. Watts *et al*., The 2020 report of The Lancet Countdown on health and climate change: Responding to converging crises. *Lancet* **397**, 129–170 (2021).
2. C. Mora *et al*., Global risk of deadly heat. *Nat. Clim. Chang.* **7**, 501 (2017).
3. T. K. R. Matthews, R. L. Wilby, C. Murphy, Communicating the deadly consequences of global warming for human heat stress. *Proc. Natl. Acad. Sci. U.S.A.* **114**, 3861–3866 (2017).
4. G. A. Meehl, C. Tebaldi, More intense, more frequent, and longer lasting heat waves in the 21st century. *Science* **305**, 994–997 (2004).
5. E. D. Coffel, R. M. Horton, A. De Sherbinin, Temperature and humidity based projections of a rapid rise in global heat stress exposure during the 21st century. *Environ. Res. Lett.* **13**, 014001 (2017).
6. G. Manoli *et al*., Magnitude of urban heat islands largely explained by climate and population. *Nature* **573**, 55–60 (2019).
7. E. D. Coffel, A. de Sherbinin, R. M. Horton, K. Lane, The science of adaptation to extreme heat. *Resilience* (2018).
8. H. Wouters *et al*., Heat stress increase under climate change twice as large in cities as in rural areas: A study for a densely populated midlatitude maritime region. *Geophys. Res. Lett.* **44**, 8997–9007 (2017).
9. T. R. Oke, Canyon geometry and the nocturnal urban heat island: Comparison of scale model and field observations. *J. Climatol.* **1**, 237–254 (1981).
10. E. Day, S. Fankhauser, N. Kingsmill, H. Costa, A. Mavrogianni, Upholding labour productivity under climate change: An assessment of adaptation options. *Clim. Policy* **19**, 367–385 (2019).
11. M. Burke, S. M. Hsiang, E. Miguel, Global non-linear effect of temperature on economic production. *Nature* **527**, 235–239 (2015).
12. T. A. Carleton *et al*., *Valuing the global mortality consequences of climate change accounting for adaptation costs and benefits (No. w27599)* (National Bureau of Economic Research, Chicago, 2020).
13. T. Chakraborty, A. Hsu, D. Manya, G. Sheriff, Disproportionately higher exposure to urban heat in lower-income neighborhoods: A multi-city perspective. *Environ. Res. Lett.* **14**, 105003 (2019).
14. E. B. Wetherley, J. P. McFadden, D. A. Roberts, Megacity-scale analysis of urban vegetation temperatures. *Remote Sens. Environ.* **213**, 18–33 (2018).
15. F. Estrada, W. J. W. Botzen, R. S. J. Tol, A global economic assessment of city policies to reduce climate change impacts. *Nat. Clim. Chang.* **7**, 403 (2017).
16. C. Tuholske, K. Caylor, T. Evans, R. Avery, Variability in urban population distributions across Africa. *Environ. Res. Lett.* **14**, 085009 (2019).
17. C. Raymond, T. Matthews, R. M. Horton, The emergence of heat and humidity too severe for human tolerance. *Sci. Adv.* **6**, eaaw1838 (2020).
18. A. M. Broadbent, E. S. Krayenhoff, M. Georgescu, The motley drivers of heat and cold exposure in 21st century US cities. *Proc. Natl. Acad. Sci. U.S.A.* **117**, 21108–21117 (2020).
19. J. K. Vanos, J. W. Baldwin, O. Jay, K. L. Ebi, Simplicity lacks robustness when projecting heat-health outcomes in a changing climate. *Nat. Commun.* **11**, 6079 (2020).
20. E. C. De Perez *et al*., Global predictability of temperature extremes. *Environ. Res. Lett.* **13**, 054017 (2018).
21. B. C. O'Neill *et al*., Achievements and needs for the climate change scenario framework. *Nat. Clim. Chang.* **10**, 1–11 (2020).
22. T. T. Smith, B. F. Zaitchik, J. M. Gohlke, Heat waves in the United States: Definitions, patterns and trends. *Clim. Change* **118**, 811–825 (2013).
23. A. Verdin *et al*., Development and validation of the CHIRTS-daily quasi-global high-resolution daily temperature data set. *Sci. Data* **7**, 303 (2020).
24. C. Funk, P. Peterson, S. Peterson, S. Shukla, A high-resolution 1983–2016 Tmax climate data record based on infrared temperatures and stations by the climate hazard center. *J. Clim.* **32**, 5639–5658 (2019).
25. N. Watts *et al*., The 2019 report of The Lancet Countdown on health and climate change: Ensuring that the health of a child born today is not defined by a changing climate. *Lancet* **394**, 1836–1878 (2019).
26. H. Hersbach *et al*., The ERA5 global reanalysis. *Q. J. R. Meteorol. Soc.* **146**, 1999–2049 (2020).
27. United Nations, Department of Economic and Social Affairs, Population Division, *World Urbanization Prospects: The 2018 Revision* (Online Edition, 2018).
28. S. Russo, J. Sillmann, A. Sterl, Humid heat waves at different warming levels. *Sci. Rep.* **7**, 7477 (2017).
29. A. J. Florczyk *et al*., *Description of the GHS Urban Centre Database* **2015**, 10.2760/037310 (2019).
30. ISO, *ISO 7243: Ergonomics of the Thermal Environment—Assessment of Heat Stress Using the WBGT (Wet Bulb Globe Temperature) Index* (Int Org Standard, Geneva Switzerland, 2017).
31. NOAA, The heat index equation. https://www.wpc.ncep.noaa.gov/html/heatindex_equation.shtml. Accessed 4 April 2020.
32. K. R. Spangler, K. R. Weinberger, G. A. Wellenius, Suitability of gridded climate datasets for use in environmental epidemiology. *J. Expo. Sci. Environ. Epidemiol.* **29**, 777–789 (2019).
33. A. A. Scott, D. W. Waugh, B. F. Zaitchik, Reduced Urban Heat Island intensity under warmer conditions. *Environ. Res. Lett.* **13**, 064003 (2018).
34. M. Georgescu, P. E. Morefield, B. G. Bierwagen, C. P. Weaver, Urban adaptation can roll back warming of emerging megapolitan regions. *Proc. Natl. Acad. Sci. U.S.A.* **111**, 2909–2914 (2014).
35. K. Parsons, Heat stress standard ISO 7243 and its global application. *Ind. Health* **44**, 368–379 (2006).
36. S. S. Cheung, J. K. W. Lee, J. Oksa, Thermal stress, human performance, and physical employment standards. *Appl. Physiol. Nutr. Metab.* **41**, S148–S164 (2016).
37. B. Pradhan *et al*., Heat stress impacts on cardiac mortality in Nepali migrant workers in Qatar. *Cardiology* **143**, 37–48 (2019).
38. A. Verdin, K. Grace, F. Davenport, C. Funk, G. Husak, Can we advance individual-level heat-health research through the application of stochastic weather generators? *Clim. Change* **164**, 7 (2021).
39. NWS Internet Services Team, Excessive heat warning. https://w1.weather.gov/glossary/index.php?word=Excessive+Heat+Warning. Accessed 8 March 2021.
40. G. Rohat, J. Flacke, A. Dosio, H. Dao, M. Maarseveen, Projections of human exposure to dangerous heat in african cities under multiple socioeconomic and climate scenarios. *Earths Futur.* **121**, 1111 (2019).
41. P. Wallemacq, R. Below, D. McLean, *Economic Losses, Poverty & Disasters (1998 - 2017)* (UNISDR/CRED, 2018).
42. R. Hoffmann, A. Dimitrova, R. Muttarak, J. Crespo Cuaresma, J. Peisker, A meta-analysis of country-level studies on environmental change and migration. *Nat. Clim. Chang.* **10**, 904–912 (2020).
43. A. Zimmer *et al*., Dynamics of population growth in secondary cities across southern Africa. *Landsc. Ecol.* **35**, 2501–2516 (2020).
44. J. V. Henderson, A. Storeygard, U. Deichmann, Has climate change driven urbanization in Africa? *J. Dev. Econ.* **124**, 60–82 (2017).
45. R. Black, S. R. G. Bennett, S. M. Thomas, J. R. Beddington, Climate change: Migration as adaptation. *Nature* **478**, 447–449 (2011).
46. S. Kumar, India's heat wave and rains result in massive death toll. *Lancet* **351**, 1869 (1998).
47. T. E. Bernard, I. Iheanacho, Heat index and adjusted temperature as surrogates for wet bulb globe temperature to screen for occupational heat stress. *J. Occup. Environ. Hyg.* **12**, 323–333 (2015).
48. C. P. Kelley, S. Mohtadi, M. A. Cane, R. Seager, Y. Kushnir, Climate change in the Fertile Crescent and implications of the recent Syrian drought. *Proc. Natl. Acad. Sci. U.S.A.* **112**, 3241–3246 (2015).
49. F. G. Kuglitsch *et al*., Heat wave changes in the eastern Mediterranean since 1960: Heat waves in the Eastern Mediterranean. *Geophys. Res. Lett.* **37**, 529 (2010).
50. D. Helman, B. F. Zaitchik, C. Funk, Climate has contrasting direct and indirect effects on armed conflicts. *Environ. Res. Lett.* **15**, 104017 (2020).
51. H. Buhaug, Climate-conflict research: Some reflections on the way forward. *Wiley Interdiscip. Rev. Clim. Change* **6**, 269–275 (2015).

52. R. G. Steadman, The Assessment of Sultriness, Part II: Effects of wind, extra radiation and barometric pressure on apparent temperature. *J. Appl. Meteorol. Climatol.* **18**, 874–885 (1979).
53. A. Casanueva *et al*., Overview of existing heat-health warning systems in Europe. *Int. J. Environ. Res. Public Health* **16**, 2657 (2019).
54. 1990-6-26 Phoenix, AZ Weather History. https://www.wunderground.com/history/daily/KPHX/date/1990-6-26. Weather Underground. Accessed 20 June 2021.
55. A. Minkler, At 118 degrees, Thursday heat in Phoenix breaks daily record set in 1934. The Arizona Republic. https://www.azcentral.com/story/news/local/phoenix-weather/2020/07/30/record-breaking-temperatures-and-heat-forecast-phoenix-area/5544421002. Accessed 18 June 2021.
56. L. E. Watkins *et al*., Extreme heat vulnerability in Phoenix, Arizona: A comparison of all-hazard and hazard-specific indices with household experiences. *Appl. Geogr.* **131**, 102430 (2021).
57. W.-C. Chuang, P. Gober, Predicting hospitalization for heat-related illness at the census-tract level: Accuracy of a generic heat vulnerability index in Phoenix, Arizona (USA). *Environ. Health Perspect.* **123**, 606–612 (2015).
58. T. Kjellstrom, Impact of climate conditions on occupational health and related economic losses: A new feature of global and urban health in the context of climate change. *Asia Pac. J. Public Health* **28**, 28S–37S (2016).
59. P. Zhang, O. Deschenes, K. Meng, J. Zhang, Temperature effects on productivity and factor reallocation: Evidence from a half million Chinese manufacturing plants. *J. Environ. Econ. Manage.* **88**, 1–17 (2018).
60. World Bank, Population living in slums (% of urban population) | Data (2019). https://data.worldbank.org/indicator/EN.POP.SLUM.UR.ZS. Accessed 26 October 2019.
61. S. Fox, Urbanization as a global historical process: Theory and evidence from sub-Saharan Africa. *Popul. Dev. Rev.* **38**, 285–310 (2012).
62. R Rohde *et al*., Berkeley Earth temperature averaging process. Geoinfor Geostat. *An Overview* **1**, 2, 10.4172/2327-4581.1000103 (2013).
63. J. Sheffield, G. Goteti, E. F. Wood, Development of a 50-year high-resolution global dataset of meteorological forcings for land surface modeling. *J. Clim.* **19**, 3088–3111 (2006).
64. D. Bolton, The computation of equivalent potential temperature. *Mon. Weather Rev.* **108**, 1046–1053 (1980).
65. A. Cattaneo, A. Nelson, T. McMenomy, Global mapping of urban–rural catchment areas reveals unequal access to services. *Proc. Natl. Acad. Sci. U.S.A.* **118**, e2011990118 (2021).
66. D. L. Balk, M. R. Montgomery, Guest editorial: "Spatializing demography for the urban future. *Spat. Demogr.* **3**, 59–62 (2015).
67. K. Parsons, *Human Thermal Environments: The Effects of Hot, Moderate, and Cold Environments on Human Health, Comfort, and Performance* (CRC Press, ed. 3, 2014).
68. G. D. Bynum *et al*., Induced hyperthermia in sedated humans and the concept of critical thermal maximum. *Am. J. Physiol.* **235**, R228–R236 (1978).
69. S. S. Cheung, T. M. McLellan, Heat acclimation, aerobic fitness, and hydration effects on tolerance during uncompensable heat stress. *J Appl Physiol (1985)* **84**, 1731–1739 (1998).
70. A. Bouchama *et al*., Inflammatory, hemostatic, and clinical changes in a baboon experimental model for heatstroke. *J Appl Physiol (1985)* **98**, 697–705 (2005).
71. K. B. Pandolf, R. F. Goldman, Convergence of skin and rectal temperatures as a criterion for heat tolerance. *Aviat. Space Environ. Med.* **49**, 1095–1101 (1978).
72. S. C. Sherwood, M. Huber, An adaptability limit to climate change due to heat stress. *Proc. Natl. Acad. Sci. U.S.A.* **107**, 9552–9555 (2010).
73. M. Burke *et al*., Higher temperatures increase suicide rates in the United States and Mexico. *Nat. Clim. Chang.* **8**, 723–729 (2018).
74. S. M. Hsiang, K. C. Meng, M. A. Cane, Civil conflicts are associated with the global climate. *Nature* **476**, 438–441 (2011).
75. G. Ceccherini, S. Russo, I. Ameztoy, Heat waves in Africa 1981–2015, observations and reanalysis. *Nat. Hazards* **17**, 115–125 (2017).
76. C. Tuholske *et al*., Global high resolution daily urban extreme heat exposure (UEH-Daily) 1983 - 2016. Socioeconomic Data and Applications Center (SEDAC). https://ciesin.columbia.edu/data/global-ueh-daily/. Deposited 9 September 2021.